Experimental-based Subsystem Models for Simulation of Heterogeneous Optical Networks

Eduardo Magalhães, Miquel Garrich, Uiara Moura, Lara Nascimento, Juliano Oliveira
Optical System Division, CPqD – Telecom & IT Solutions, Campinas, Brazil, {eduardom}@cpqd.com.br

Aldário Bordonalli
DMO, FEEC, UNICAMP, Campinas, Brazil, {aldario}@dmo.fee.unicamp.br

***Abstract*— This work presents and analyzes experimental-based subsystem models for Erbium doped fiber amplifiers (EDFAs) and wavelength selective switches (WSSs) under operation in a metropolitan optical network testbed. Firstly, the performance of the EDFAs and two gain control types are analyzed in a heterogeneous experimental setup with lightpaths modulated at 10G/100G/200G. Secondly, the WSS optical shape filter is experimentally characterized. Subsequently, simulation models are proposed accordingly to the experimental data obtained from the experimental setups. Results of output power and spectrum shape for both amplifiers under test showed good agreement between simulation and experiment. In addition, the optical signal-to-noise ratio (OSNR) for all channels was also analyzed and it was obtained error values bellow 1 dB, which are within an acceptable error margin. The developed sub-system models will provide greater flexibility to simulate different network scenarios and enable the development and validation of future optical network intelligence algorithms.**

***Index Terms*—** Elastic optical networking; Flexible optical networking; Optical networking; Cognitive optical networks.

I. INTRODUCTION

The progress in the last years on Information and Communications Technologies (ICTs) has shaped society's way of living in lots of aspects. Clear examples are the emergence of new services and applications such as video-on-demand, high-definition TV and cloud computing, supported by either wireless or Fiber-To-The-x (FTTx) based broadband access technologies [1]. Therefore, network operators must overcome the exponential bandwidth demand driven by these bandwidth-hungry services, applications and access technologies. In this context, two main technology fields are also evolving to cope with such challenging scenario.

On the one hand, transmission systems are using high order modulation formats to guarantee high spectral efficiency. For instance, quadrature phase-shift keying (QPSK), 16-ary quadrature amplitude modulation (16-QAM), or optical orthogonal frequency-division multiplexing (OFDM), are common ways to improve the usage of the available spectrum resources [2]–[4]. However, it is well known that bit loading higher than that for QPSK/QAM/OFDM poses constraints in the optical signal-to-noise ratio (OSNR) at the receiver [5].

On the other hand, optical networks have capitalized on the advent of wavelength selective switches (WSS) that enable unprecedented levels of elasticity and dynamicity. In more detail, elastic and dynamic optical networks are becoming a reality in the telecommunication scenario, especially for wavelength division multiplexed core nodes, and, in some cases, for metro- and aggregation-nodes

Brazilian Microwave and Optoelectronics Society-SBMO *received 16 May 2014; for review 20 May 2014; accepted 23 Oct 2014*
Brazilian Society of Electromagnetism-SBMag *ISSN 2179-1074*

[6]. Therefore, considering the progress on optical transmission and networking, current links/systems are rapidly evolving from point-to-point links to complex meshed networks. Moreover, for network applications and services to provide full and appropriate utilization of the available resources, different requirements have to be fulfilled motivating the research on active and programmable networks since the early 1990s. However, networks are still managed by technicians with in-site manual interventions and operations. Current optical networks perform reactive adaptation by responding to changes in the environment after a problem has occurred [7]. This occurs due the network lack of awareness, self-knowledge, and proper aim targets with which would be suitable to apply actions that minimize failure restoration times, guarantee low blocking ratios, increase resources efficiency, and thus, achieve enhanced network performance.

In this challenging context, several works in the literature are proposing architectures, strategies, techniques and sub-systems that operate in an autonomic and/or cognitive way. In particular, current research works investigate adaptive optical transceivers, able to sense the channel conditions and to adapt their operation parameters to extend reach and reduce power consumption [8]. Caballero et al. [9] propose a technique to predict whether optical channels fulfill quality of transmission (QoT) requirements supporting impairment-aware networking. Note that the technique proposed in [9] is validated by means of a simulation platform that considers experimental data as data/knowledge base to apply the cognitive QoT estimator. Similarly, Gonzalez et al. [10] demonstrate a novel cognitive receiver for modulation format recognition over radio-over-fiber links. Additionally, an European project known as Cognitive Heterogeneous Reconfigurable Optical Network (CHRON) developed a testbed of a cognitive network able to self-configure and self-optimize to efficiently use available resources [11]. As basis to perform and propose new optimization approaches in scenarios with all this complexity, it is crucial to have a simulation tool with proper and realistic optical network model able to provide an environment that is capable of simulating without physical resources limitations and able to integrate proof-of-concept features.

This work is based on experimental results reported in [12-14]. In [12] we introduced a global (end-to-end) ROADM-based spectrum equalizer algorithm running over DWDM networks on SDN architecture. Moreover, in [13] we experimentally demonstrate the benefits of global WSS-based spectrum equalization for multiple ROADMs in cascade and introduced three equalization strategies to enable OSNR enhancement in a SDN metropolitan mesh optical network test-bed. Finally, in [14] we demonstrated an adaptive gain control for EDFA operation in real-time GMPLS controlled heterogeneous optical testbed with 10G/100G/200G/400G lightpaths.

In this paper, we present experimental-based models to simulate optical links, providing adaptive set point control of EDFAs and WSS models which enable the development and validation of future optical network intelligence algorithms. To achieve that, we first review our experiments of EDFA adaptive gain control (AdGC) and ROADM characterization focusing on the sub-systems involved for later modelling. Subsequently, we validate the simulation algorithms and models written for

Brazilian Microwave and Optoelectronics Society-SBMO *received 16 May 2014; for review 20 May 2014; accepted 23 Oct 2014*
Brazilian Society of Electromagnetism-SBMag *ISSN 2179-1074*

commercial simulation softwares. Initially, we design the EDFA automatic gain control loop (AGC) and then we integrate the EDFA with the ADGC. Secondly, we test and validate with random initial conditions for transmitted WDM signals and several modulation formats. As a result, this model was able to establish near optimum operating points for the EDFAs that could guarantee high performance connection (OSNR error within ±1 dB in relation to experimental results) between particular network nodes, even if the initial conditions are abruptly changed. It is important to point out that the implementation of cognitive techniques is out of the scope of this paper. This work concentrates on the sensing and acting tasks as preliminary steps for learning techniques that will be considered in future work.

The paper is organized as follows. Sec. II presents the experimental setup and details the EDFA and WSS experimental characterization, respectively. Sec. III details the implementation model of each simulated device. In Sec. IV describes the test cases and Sec. V shows the results and discuss them for each figure of merit under analysis. Several remarks and conclusions are provided in Sec. VI.

II. CPqD's Metropolitan Optical Network Testbed

In this section, we first describe CPqD's metropolitan optical network testbed. Then we detail in two subsections the setups for EDFA and WSS characterization, respectively. Fig. 1(a) shows the

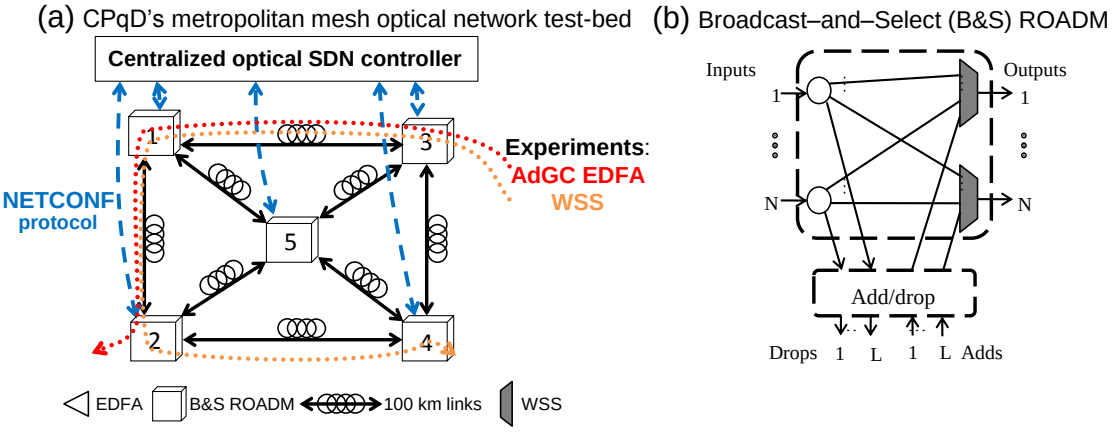

Fig. 1. (a) CPqD's metropolitan mesh optical network and (b) B&S ROADM structure.

metropolitan optical testbed.

The metropolitan optical mesh network test-bed at CPqD consists of a central ROADM of degree 4 and four edge ROADMs of degree 3 that support flexible-grid channel allocation. All ROADMs in the network are based on a broadcast-and-select as shown in Fig. 1(b). All ROADMs are built without add/drop structure (i.e. one add and one drop port are available per degree, colored and directional). Connectivity between ROADMs is provided with 100-km SSMF (G.652) links and two EDFAs. In each node runs a node controller daemon implementing a ROADM abstraction layer based in the YANG [15] language. All these optical network subsystems provide to the centralized software defined network (SDN) controller monitoring data and configuration information via NETCONF [16]. On the one hand, optical channel monitor (OCM) modules gather optical spectrum monitoring data at

each ROADM and photodetectors provide total optical power data at each EDFA. On the other hand, the network control parameters include WSS switching, EDFA gain set-point, variable optical attenuators (VOA) and 100G transmitter control.

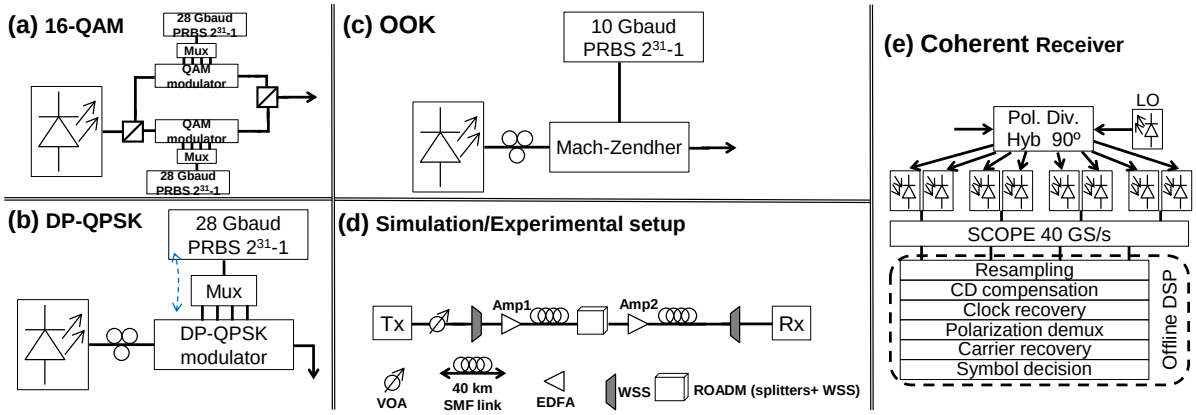

Fig. 2. (a)16-QAM, (b) DP-QPSK, (c) OOK transmitters, (d) general overview of the simulated/experimental setup and (e) coherent receiver.

A. Experimental setup for EDFA characterization

This section presents the experimental scenario used to evaluate the performance enhancement algorithm which controls the EDFAs' operating points of the experimental optical network testbed reported in [14]. Firstly, three different modulation formats were distributed at five different wavelengths: three 10 Gb/s on-off keying (OOK) with chromatic dispersion (CD) pre-compensation (1555.75, 1535.82 and 1531.12 nm, respectively); a 112 Gb/s dual polarization (DP) QPSK (1550.92 nm); and 224 Gb/s pre-filtered DP-16QAM (1557.36 nm), as shown in Fig 2 (a)-(c).

A scenario with five WDM transmitters allocated at C band with equalized power levels of -20 dBm (per channel) at the link input were considered, similarly to the experiment reported in [13]. Table 1 summarizes the ITU-T grid channels used and their respective modulation formats.

The 224 Gb/s DP-16QAM signal was obtained using a 500-kHz linewidth laser centered at 1557.36 nm. A polarizing beam splitter (PBS) separated the laser signal into two orthogonal polarization state signals, which were then individually modulated by QAM modulators driven by four 28 Gb/s sequence generators (pseudorandom pattern with 2^{30}-1 bits). After the modulators, the signals were combined again by a polarization beam combiner (PBC) and sent over the transmission link. Fig. 2 (a) presents the 16-QAM transmitter.

For the 112 Gbit/s DP-QPSK scheme, four 28 Gbit/s decorrelated lines (31th-order pseudorandom binary sequence) drove two IQ modulators. These four electrical signals modulate phase and quadrature in both polarizations by using IQ modulators based on Mach-Zehnder interferometers and polarization rotators as shown in Fig. 2 (b). Finally, the on-off keying (OOK) carriers used a conventional modulation scheme based on a single Mach-Zehnder modulator (Fig. 2 (c)). Fig. 3 shows the optical spectrum at the link input.

Brazilian Microwave and Optoelectronics Society-SBMO *received 16 May 2014; for review 20 May 2014; accepted 23 Oct 2014*
Brazilian Society of Electromagnetism-SBMag *ISSN 2179-1074*

Then, two EDFAs were used to compensate signal losses over the optical link. The experimental setup was composed of 3 reconfigurable optical add/drop multiplexer (ROADM) nodes, represented by 3 WSSs, and 2 fiber spans of 100 km, as in Fig. 1 (a) (dotted red line). An adaptation of the generalized multi-protocol label switching (GMPLS) control plane used to read and act on real-time optical network elements and configured by the optical link management protocol (OLMP) through an optical service channel (1510 nm). To evaluate EDFA's control with different situations, physical layer impairments (PLI) were intentionally added by means of a variable optical attenuator (VOA) at the input of Amplifier 1 (Amp 1). The EDFA gain-adjustments via adaptive control was applied to the power amplifier (Amp 1) and in-line amplifier (Amp 2) used in the link. At **receiver** all channels were demultiplexed and the ones using QPSK and 16-QAM modulation formats were recovered by using coherent digital detection (Fig. 2 (e)), in accordance with the simulated scheme described later in this section. The experimental electrical outputs from the balanced photodetectors at the receiver where sampled by a real-time oscilloscope, acquiring 40k samples per XYIQ electrical line at 80GS.

TABLE I - CHANNELS CHARACTERISTICS

Channels	Wavelength (nm)	Bit-rate (Gbps)	ITU-T grid	Mod. format
CH1	1557.36	224	C25	DP-16-QAM
CH2	1555.75	10	C27	NRZ-OOK
CH3	1550.92	112	C33	DP-QPSK
CH4	1535.82	10	C52	NRZ-OOK
CH5	1531.12	10	C58	NRZ-OOK

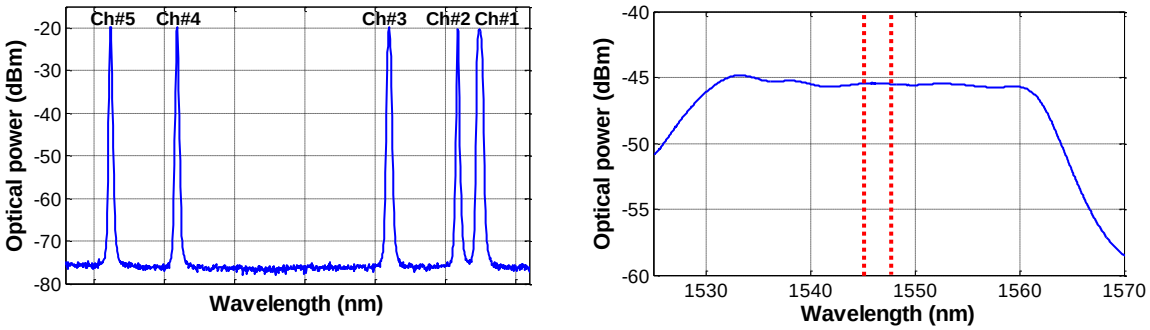

Fig. 3. Experimental input signals to (a) EDFA AdGC and (b) WSS models, respectively.

B. Experimental setup for WSS characterization

WSS are key components in dynamic optical networks, they allowed the consolidation of optical dynamic networks in the telecom scenario, especially for complex mesh topologies in particular with optical spectrum equalization. Reconfigurable optical add/drop multiplexers (ROADMs), usually based on wavelength selective switches (WSSs), are key elements since they route signals directly in the optical domain. Proper global operation of ROADMs under a SDN controller may provide benefits in terms of OSNR allowing higher network capacity, longer transmission reaches and

Brazilian Microwave and Optoelectronics Society-SBMO *received 16 May 2014; for review 20 May 2014; accepted 23 Oct 2014*
Brazilian Society of Electromagnetism-SBMag *ISSN 2179-1074*

flattened spectral shapes for proper amplification operation. Indeed, SDN-enabled global algorithms may offer end-to-end performance improvements against local optimizations of network elements applied in a stand-alone fashion [12]. In [13] three equalization strategies are proposed to offer high OSNR enhancement and longer reach suitable for future high SE transmission systems. In this way, to obtain an accurate WSS model an optical response of WSS optical filtering is required for proper simulation results.

This section presents an experimental characterization of bandpass filters from 12.5 to 100 GHz used in flexible grid WSS. To do that an EDFA generates the optical spectrum to seed WSS input and the results are analyzed by an optical spectrum analyzer (OSA).

For the flexible DWDM grid, the allowed frequency slots have a nominal central frequency (in THz) defined by: 193.1 THz + (n x 0.00625 THz), where "n" is a positive or negative integer including 0, and 0.00625 THz (6.25 GHz) is the nominal central frequency granularity and a slot width is defined by: (12.5 x m), where "m" is a positive integer and 12.5 is the slot width granularity in GHz. Slices from 12.5 to 100 GHz in the amplified spontaneous emission (ASE) flat region was chosen to be analyzed shown in Fig. 3(b) (red line dotted).

After, to model the curves "nutonian EUREQA II (code name formulize)" was used [16]. EUREQA uses a genetic algorithm search to determine an analytic function. The program receives as data input a vector of frequencies (normalized) *w* a vector of amplitudes (in linear scale) *x*. An analytical function $x = f(w)$ is seek and defined by a model with a number of coefficients that combines several functions (building blocks) and the coefficients values.

As a result, the filters of 12.5 GHz to 100 GHz (composed of 3 or more slices) having a flat top, are well approximated by a model of the type: tanh (c1 * gauss (c2 * (w - c3)^2)) . where the coefficient c2 is related to the width of the filter and c3 with the center frequency.

III. SIMULATION MODELS

This section describes the models used for each optical component OptiSystem© and Matlab© softwares were used to support all simulations. Firstly, we describe the transmitter models for each modulation format and the variable optical attenuator and optical fiber models. Additionally, we describe the ROADM model in particular WSS model. Moreover, EDFA AGC model is describe as well as adaptive gain control model. Finally, we describe the coherent receiver with the digital signal processing setup algorithms used.

A. Transmitter models

The transmitter models simulated are based on the same structure presented previously in section II. Fig. 4(a) shows the general 112G DP-QPSK transmitter and in detail fig. 4(b) shows the DP-QPSK modulator. Additionally, in fig. 4(c) shows the internal structure with two Mach-Zhender modulators. Finally, figs. 4 (d) and (e) shows the 16-QAM and OOK transmitters, respectively.

In fig. 4(a) the DP-QPSK transmitter is composed of four ideal PRBS lines. Each one line pass

Brazilian Microwave and Optoelectronics Society-SBMO *received 16 May 2014; for review 20 May 2014; accepted 23 Oct 2014*
Brazilian Society of Electromagnetism-SBMag *ISSN 2179-1074*

through an NRZ driver. The outputs were amplified by 32-GHz bandwidth drivers with amplitude output of 7.0Vpp. These four lines were sent to two QPSK modulators with Vπ of 3.5V and 23-GHz bandwidth as shown in Fig. 4(b). Fig. 4(c) shows each QPSK modulator internally composed by two Mach-Zehnder modulators.

In Fig. 4(d) the 16-QAM transmitter is composed by a PBS which separates the laser signal into two orthogonal polarization state signals, which were then individually modulated by QAM modulators driven by four 28 Gb/s PRBS line electrically encoded by NRZ signals with a 500 mVpp (amplitude peak-to-peak). After at modulators output, the signals were combined again with a PBC. Finally, in Fig. 4(e) the OOK transmitter is composed by a 10 Gb/s PRBS line is encoded by a NRZ driver that feeds a Mach-Zehnder modulator.

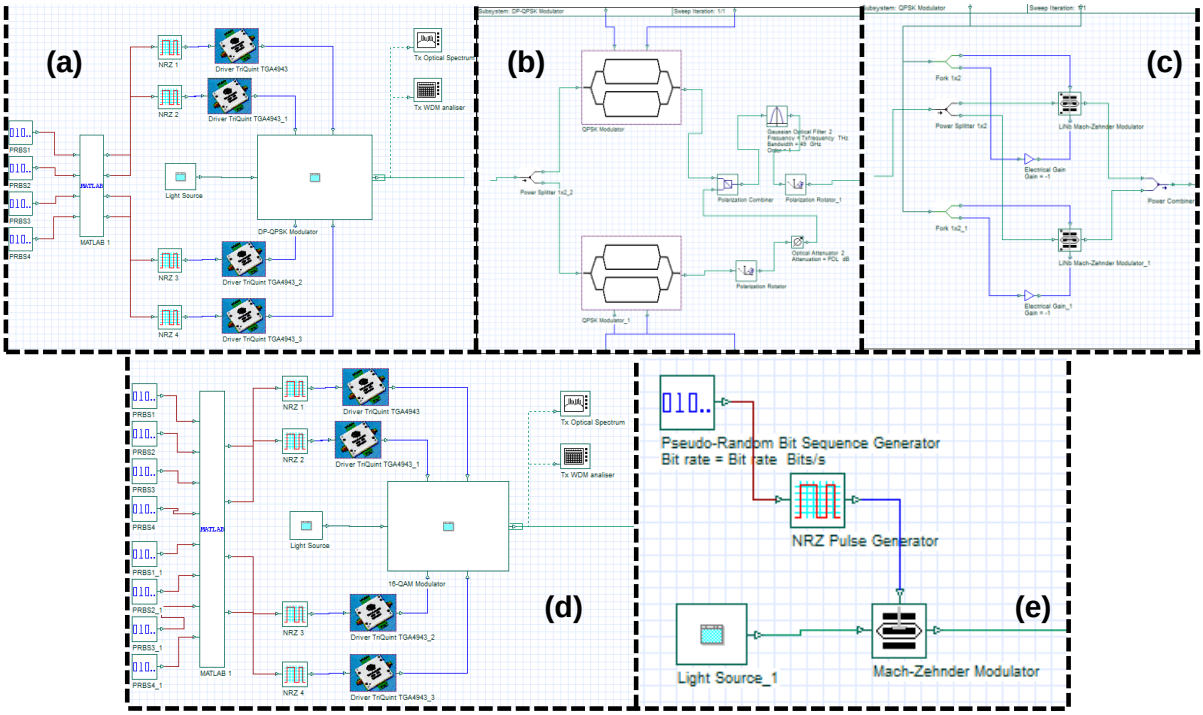

Fig. 4. (a) 112G DP-QPSK transmitter, (b) DP-QPSK modulator, (c) QPSK modulator in detail, (d) 16-QAM transmitter and (e) OOK respectively.

B. Variable optical attenuator and optical fiber models

Further, to simulate the effects of link attenuation, a variable optical attenuator (VOA) was inserted before Amplifier 1 (Amp 1). For this purpose, optical signal attenuation can be obtained:

$$\vec{E}_{outX,Y}(t) = \vec{E}_{inX,Y}(t)10^{-\alpha/20} \tag{1}$$

where $\vec{E}_{X,Y}(t)$ is the electric field vector (polarization in both X and Y) and α is the attenuation (dB). The attenuation values used were 0, 5, and 10 dB. Moreover, the optic fiber model used simulates the propagation of the electric field in a single-mode fiber with dispersion and nonlinear effects considered from the numerical integration of the nonlinear Schrödinger equation (NLS) [18].

C. ROADM model

ROADMs are key network elements, switching directly in the optical domain, allowing for an

active and flexible control of wavelength insertion and removal. Broadcast-and-select (B&S) and route-and-select (R&S) are the two main structures used in ROADM internal structure. The classical B&S (Fig. 1(b)) of degree N is implemented using N splitters connected in a full mesh to N WSSs that filter the undesired lightpaths at each output. On the other hand, the R&S of degree N is composed of two stages of N WSSs. The first stage of WSSs routes (i.e. switches and filters) the express lightpaths towards the outputs and the dropped lightpaths towards the add-drop bank. Lightpaths are then filtered again at the select stage of WSSs guaranteeing lower loss and higher isolation compared to the Broadcast-and-Select express bank, but at the cost of a higher energy consumption [19].

1) Wavelength selective switch model

We simulate ROADM with a B&S structure composed of a power splitter followed by a WSS represented by the flowchart in Fig. 5. In this B&S structure a stage composed of one power splitter per input sends spectral attenuated copies of the incoming signal to all WSS switches and to the drop ports. A WSS per output is used to filter and attenuate if necessary the optical channels. At the same time the add port also send signals to the WSS switches. Wavelengths can be freely switched from one degree to another provided that its frequency is available in the destination port. This operation is commonly referred as express path switching.

It is known that to perform optical switching functions and wavelength insertion/removal, dynamic optical filtering is required [6]. Therefore, to simulate the experimental optical filtering response of the WSS operating at both 50 and 100 GHz channel spacing, an initial investigation was carried out to determine the closest filter response from different filter types and orders as previously discussed in section II. Table 2 presents the best fitting obtained for the WSS response. For instance, a 50 Ghz bandwidth allocated in the WSS its necessary a 2nd Gaussian filter with 44 GHz of 3-dB bandwidth.

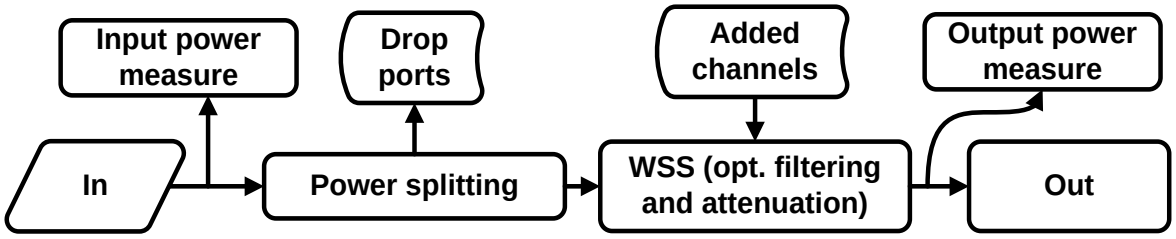

Fig. 5. ROADM operation flowchart.

TABLE II - WSS EXPERIMENTAL PERFORMANCE

Bandwidth	100 GHz	50 GHz
Type	Gaussian	Gaussian
Filter order	4	*2*
3 dB bandwidth	± 46.68 GHz	*± 22 GHz*

Brazilian Microwave and Optoelectronics Society-SBMO *received 16 May 2014; for review 20 May 2014; accepted 23 Oct 2014*
Brazilian Society of Electromagnetism-SBMag *ISSN 2179-1074*

D. EDFA AGC model

In the following, we detail the EDFA AGC model based on experimental characterization for simulation purposes. Firstly, we detail the EDFA model implemented in Optisystem with real parameters based on experimental measures. Fig. 6 (a) and (b) depicts the erbium doped fiber amplifier (EDFA) optical circuits and their sub-devices, respectively. All EDFAs in Fig. 1(a) were designed to provide high flatness gain and low noise figure at 17 dB of set-point gain. Each EDFA optical circuit consists of a single stage 14-m long erbium doped fiber (EDF) with co-propagating pump at 980 nm and 500 mW of nominal optical power. Signal and pump powers are combined via an integrated component, which is formed by a 99/1 fiber coupler (TAP 1), an isolator (ISO) and a pump coupler (WDM), before the EDF. At the other end, an optical attenuator (ATT) is used to simulate TAP losses for output and feedback control output power monitoring.

Fig. 6 (b) depicts in detail the feed-forward based AGC scheme used for simulated EDFAs gain control. TAP 1, in Fig. 6 (a), samples the input power, which is detected by a photodetector (PD), and provides data for the feed-forward controller in Fig. 6 (b). Then, the controller acts on the pump laser (PL) bias to set the amplifier gain via pump power adjustments. However, to obtain the proper gain control, an initial optical characterization of the EDFA was necessary. This process consists of varying the EDFA optical input (in this case, composed of 40 non-modulated full C-band channels) and pump powers, measuring the respective output power levels for each setting, and determining the resulting power gain in order to calculate feed-forward coefficients that map the gain control. Indeed, the coefficients are estimated, for each gain setpoint, from those of a five order polynomial equation relating pump and input powers. Thus, for a given input power value, pump can be adjusted by the controller from the computed polynomial equation for a desired gain.

Feed-forward AGC was used in simulation due the long simulation time required to use feedback AGC in optical amplifiers through Optisystem®. Simulated feed-forward AGC runs in 18 seconds instead 1200 seconds for simulated feedback AGC.

1) Adaptive gain control model

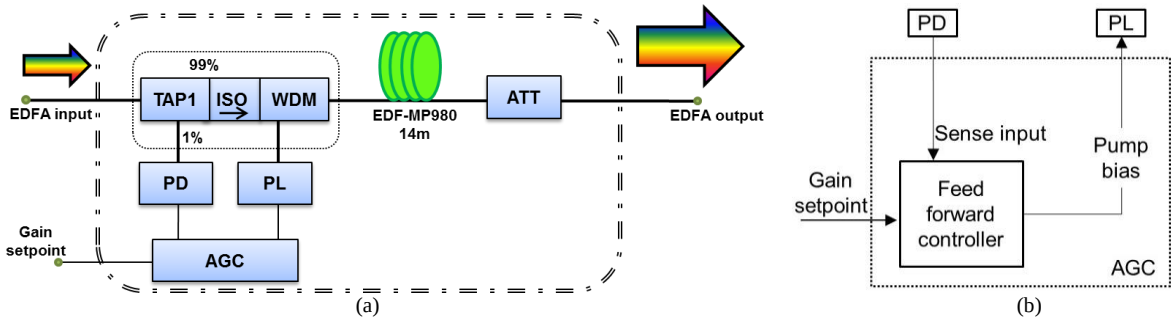

Fig. 6. (a) Simulated structure used to the erbium doped fiber amplifier and (b) its feed-forward automatic gain control block diagram.

ISSN 2179-1074

Once the EDFA gain control is established, several steps are necessary to guarantee that the EDFA gain set-point adjustment scheme is based on assumptions of being aware and adaptive. Thus, an algorithm is required to act on the EDFA operating point when the amplifier input power varies. To

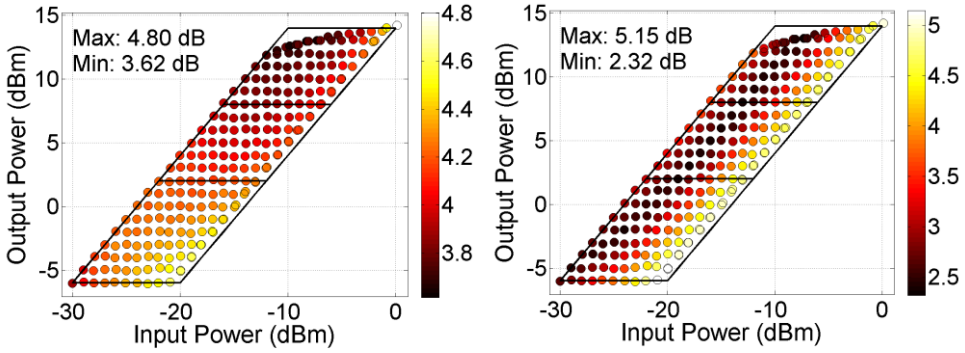

(a) (b)

Fig. 7. Power masks with information of (a) noise figure (NF) and (b) gain flatness (GF).

do so, it is essential a prior characterization, different from the one accomplished to simulated AGC in previous the section, to obtain the amplifier static parameters inside its power mask [14,20].

In this other characterization, for each pair of values of input power and gain (considering the same

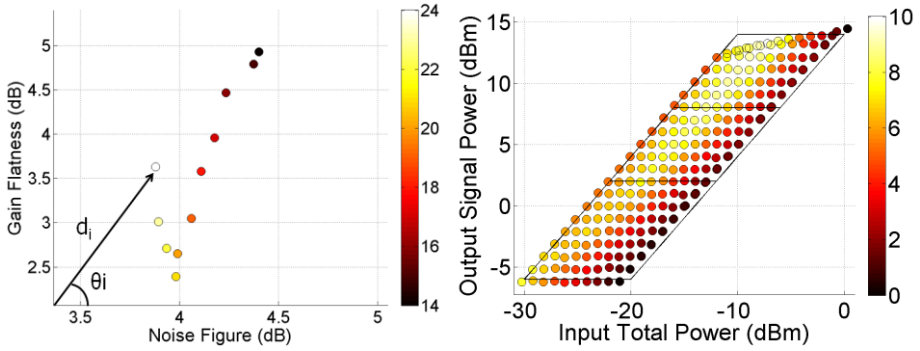

(a) (b)

Fig. 8. (a) Objective space of GF vs NF for P_{in} = -15 dBm and (b) power mask with the absolute value of the fitness function.

40 non-modulated full C-band channels), noise figure and channel power variation between the lowest and highest peak power (gain spectral flatness) are measured. The characterization results are shown in Fig. 8, which presents the amplifier power mask with information of noise figure (a) and gain flatness (b). It is possible to observe a distinct behavior for the noise figure (NF) and gain flatness (GF), which allows for determination of the best gain set point with respect to each parameter, for different input power conditions [20].

However, to determine a new operating point (target gain) for a new value of input power, noise figure and gain spectral flatness must be simultaneously optimized. To do that, an objective was plotted for each input power, with information of GF and NF on the axes, as shown in Fig. 8(a), which shows the objective space for a -15-dBm of input power, with the color chart levels related to different gain values. It can be seen that, for a given value of input power, moving from a low to a high value of target gain, noise figure and flatness tend to improve [20]. However, below NF = 4 dB,

the flatness begins to deteriorate while still reducing noise figure. It may also be noted that the points closer to the origin of the graph show a combination of improved values for noise figure and gain spectral flatness, simultaneously.

In this way, the Euclidean distance d_i between a given point and the origin can be associated with a quality function, denoted as fitness function:

$$fitness_i = \frac{1}{d_i} \angle \theta_i \tag{2}$$

where

$$d_i = \sqrt{NF_i^2 + Flatness_i^2} \tag{3}$$

and θ_i is the polar angle defined in fig. 4 and written as:

$$\theta_i = \arctan\left(\frac{NF_i}{Flatness_i}\right) \tag{4}$$

In case two points have the same distance the difference between the fitness functions would then be given by the angular coefficient (related to θ_i) defined by each line, and shown in Fig. 8(a). Thus, the EDFA operating point could be chosen in agreement with which parameter had to be selected. For example, if the noise figure is to be prioritized from the results shown in Fig. 8(a), the point with the largest angle is chosen. On the other hand, if the fitness function has to consider the gain flatness, a smaller argument should be chosen.

In (2), the value of the fitness function (complex) is inversely proportional to the distance. That is to consider that the greater the distance, the larger are the values of noise figure and spectral flatness and, consequently, lower (worse) the value of the fitness function.

By considering that a new operating point requires the noise figure and gain spectral flatness to be simultaneously optimized, the modulus of the values of the quality function can be normalized from 0 and 10, to generate a grading score for EDFA performance considerations. Thus, for each value of input and output powers, the graded converted fitness function values can be presented as an optimized power mask that takes into account the combined influences of NF and GF as in Fig 8(b). This improved power mask is used as reference for the future decisions on the EDFA performance within the network. Fig. 9 summaries the adaptive gain control operation.

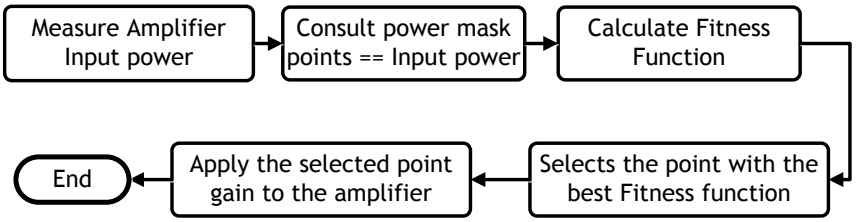

Fig. 9. Adaptive gain control flowchart.

E. Receiver model

At the receiver all 5 channels were de-multiplexed within a 100-GHz bandwidth. For the different

Brazilian Microwave and Optoelectronics Society-SBMO *received 16 May 2014; for review 20 May 2014; accepted 23 Oct 2014*
Brazilian Society of Electromagnetism-SBMag *ISSN 2179-1074*

tests carried out later, the QPSK and 16-QAM modulated channels were used as measurement references and were then individually coupled into one of the ports of a polarization-diversity 90º optical hybrid depicted in Fig. 10(a) and (b). A 150-kHz linewidth local oscillator (LO) signal was simultaneously coupled to the other hybrid port to select the channel under test via coherent intradyne detection (frequency difference of 60 MHz). The four outputs of the 90º optical hybrid were converted to the electrical domain using balanced photodiodes follow by a Gaussian low passband filter (LPF) to emulate receiver electrical signal filtering due to components limitation. To recover the transmitted information, these four electronic signals were digitally processed offline by using dedicated digital signal processing (DSP) algorithms in Matlab [21]. The DSP was set to compensate physical impairments, such as chromatic dispersion (CD) and polarization mode dispersion (PMD), phase noise and other limitations imposed by the transmitter and the receiver. Firstly, the received signals were sampled and quantized to simulate a realistic analog-to-digital conversion. After that, CD was compensated by using a static filter of finite impulse response (FIR). Then, the effects of PMD were compensated using an adaptive filtering algorithm followed by a phase estimation block. Finally, the retrieved data were compared with the four PRBS transmitted sequences to estimate the bit error rate (BER).

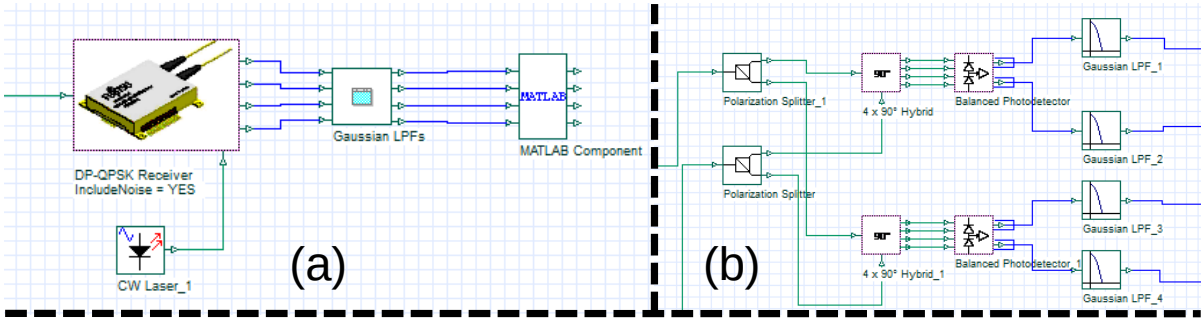

Fig. 10 (a) coherent receiver with a local oscillator and (b) receiver internal details.

IV. TEST CASES

In this section we describe the test cases used in simulations. To evaluate the simulation results, as mentioned before, the schematic diagram of Fig. 1 (a) was used (red line dotted). Note that optical parameters, such as input power and insertion loss, of all experimental devices and components were adjusted/configured during simulation for greater reliability. To calibrate and evaluate the simulation setup (shown in sec. II) against the experiment reported in [13], the adaptive EDFA algorithm was tested in several test cases. In these cases, the amplifier gain values were set to 14 and 19 dB (least minimum set-point gain to surmount the link loss). For each initial gain value for Amp 1 (G1) and Amp 2 (G2) of Fig. 1(a), physical layer impairments (PLI) were emulated via the VOA, resulting in losses (Att) of 0, 5 and 10 dB at Amp 1 input. These VOA settings result in Amp 1 input power values of -5, -10, and -15 dBm, respectively. Then, the adaptive EDFA algorithm was used to obtain a new gain set point for each test case. Table 3 summarizes the evaluated test cases. Cases 1 to 4 and 8

ISSN 2179-1074

through 10 correspond to fixed gain values of 14 and 19 dB, respectively. For test cases 5 to 7, the gains of Amp 1 and 2 were adaptively calculated for each PLI by using the adaptive EDFA algorithm.

V. RESULTS AND DISCUSSION

TABLE III - TEST CASES

Cases	Description
1	Initial G1 = 14 dB, G2 = 14 dB e Att = 0 dB
2	G1 = 14 dB, G2 = 14 dB e Att = 5 dB
3	G1 = 14 dB, G2 = 14 dB e Att = 10 dB
4	G1 = 14 dB, G2 = 14 dB e Att = 0 dB
5	AdGC G1 = 21 dB, G2 = 23 dB e Att = 0 dB
6	AdGC G1 = 21 dB, G2 = 24 dB e Att = 5 dB
7	AdGC G1 = 21 dB, G2 = 24 dB e Att = 10 dB
8	G1 = 19 dB, G2 = 19 dB e Att = 0 dB
9	G1 = 19 dB, G2 = 19 dB e Att = 5 dB
10	G1 = 19 dB, G2 = 19 dB e Att = 10 dB

G1 = setpoint gain of Amp1; G2 = setpoint gain of Amp 2; AdGC = adaptive gain calculated.

The goal of this section is twofold: First, assess the optical power and OSNR accuracy of the proposed model. Second, based on the results, estimate the signal quality under BER analysis. The study is conducted using Optisystem© and Matlab©, which runs on a commercially available computer composed of Intel Core i7, 3.4 GHz machine with 8 GB of RAM memory. Each iteration execution time was 5 minutes and the total time spent in step by simulation was 50 minutes. The components library modeled numerically by Optisystem© were used and the results were analyzed using routines implemented in Matlab©. Numerical and experimental results are compared and shown in subsequent.

As stated previously, test channels were added at amplifier #1 input, the same point were the PLI is imposed (point intentionally chosen to consider the worst case NF degradation along the amplifier chain). After the signal pass through the network, the output is collected in amplifier #2, where they are measured by an optical spectrum analyzer (OSA). The output spectra of all amplifiers are monitored by an OSA and the dynamic parameters (total input and output powers) are obtained through a centralized (directly from the amplifier) optical network control plane, which also performs the set-point gain adjustments when AdGC is running. The OSNR for all channels were measured in this experiment to evaluate the OSNR and flatness enhancement with AdGC performance (cases 5-7) compared to the case without AdGC (cases 1-4 and 8-10), i.e., with gains set to compensate span and WSS losses, and with AdGC running, which obtain the best set-point gain for each amplifier.

Fig. 11 (a)-(b) shows the results obtained regarding amplifier input and output optical powers errors, defined as in (5), for Amp 1 and 2 (shown in Fig. 2(d)), respectively. It can be noted that for both amplifiers in all the analyzed cases the curve of power input and output seems to have the same profile for both experimental and simulation.

$$\varepsilon_{Power} = Power_{experimental} - Power_{simulation} \quad (5)$$

In Fig. 11 (a), input / output power error in case 7 for Amp 1 are respectively 0.138 and 0.541 dB.

Brazilian Microwave and Optoelectronics Society-SBMO received 16 May 2014; for review 20 May 2014; accepted 23 Oct 2014
Brazilian Society of Electromagnetism-SBMag *ISSN 2179-1074*

Therefore, for the Amp 2 (Fig. 11 (b)) it can be seen that in case 3 the errors are respectively 0.13 and 0.88 dB. Thus, for the Amp 1, the maximum input power error was -0.54 dB. While for Amp 2, the maximum error was 0.88 dB. This mainly occurs due the experimental amplifier use of feedback AGC, which is very accurate due the steady state no gain error provided by the PI feedback gain control, while the simulated EDFA uses a feed-forward AGC which is more inaccurate. To avoid this

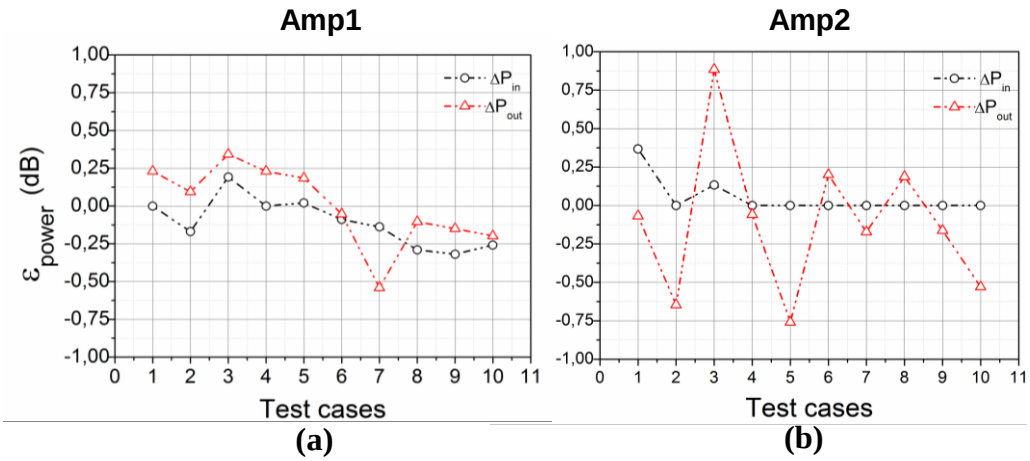

Fig. 11. Total input/output optical power with the respective errors obtained for (a)-(b) Amp1 and (c)-(d) Amp 2.

control gain error behavior a feedback AGC control method must be applied to the EDFA.

The same analysis was done considering channels OSNR and in Fig. 12 the results obtained are shown. Once again, experimental and simulated curves profiles were identical for both, Amp 1 and 2 (Fig. 12 (a) and (b), respectively). Based on the results presented in Fig. 12, we can also define the OSNR error as:

$$\varepsilon_{OSNR} = OSNR_{\exp erimental} - OSNR_{simulatior} \tag{6}$$

It can be seen in Fig. 12(a) that for case 5 the errors for all channels are respectively -0.44, 0.67, -0.04, 0.39 and 0.08 dB. We observe a maximum error of approximately ±1 dB for all cases under test. The same analysis was done for Amp 2 and the results are depicted in Fig. 7 (b). It can be seen that the error of OSNR for both amplifiers are within the same scale (1 dB). These errors can be explained

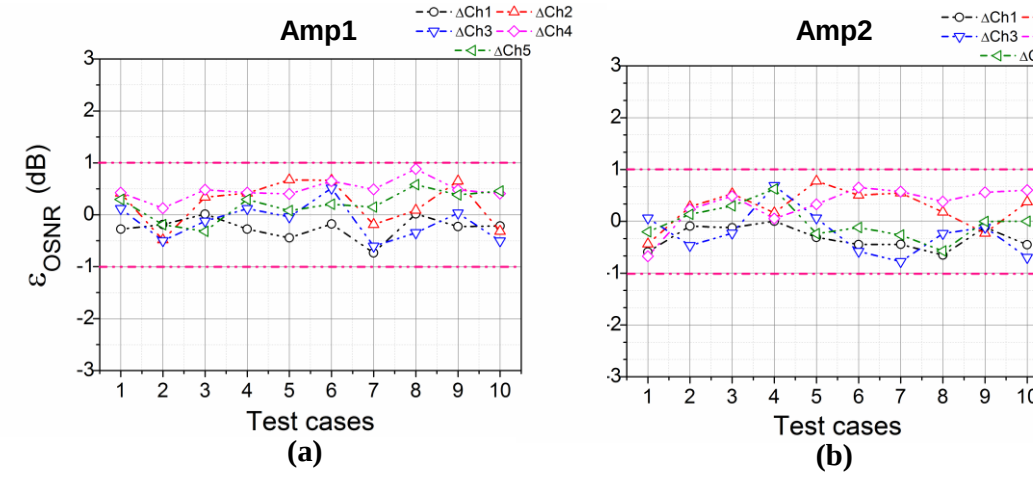

Fig. 12. Error of OSNR for all channels for (a) Amp1 and (b) Amp 2.

Brazilian Microwave and Optoelectronics Society-SBMO *received 16 May 2014; for review 20 May 2014; accepted 23 Oct 2014*
Brazilian Society of Electromagnetism-SBMag *ISSN 2179-1074*

Table IV - Results of the adaptive EDFA implementation with respect to the adaptation method.

Att.(dB)	Channel Bit rate (Gb/s)	w/o Adaptive EDFA	Adaptive EDFA
		BER	BER
5	224	Fail	OK
	10	OK	OK
	112	Fail	OK
	10	OK	OK
	10	OK	OK
10	224	Fail	OK
	10	Fail	OK
	112	Fail	OK
	10	Fail	OK
	10	Fail	OK

Case	Description	Total Power (dBm)			
		Amp1		Amp2	
		Input	Output	Input	Output
1	Início G1 = 14 dB, G2 = 14 dB e Att = 0 dB	-9.83	3.94	-10.047	3.893
2	G1 = 14 dB, G2 = 14 dB e Att = 5 dB	-14.831	-1.054	-15.291	-0.989
3	G1 = 14 dB, G2 = 14 dB e Att = 10 dB	-19.832	-6.063	-21.004	-6.133
4	G1 = 14 dB, G2 = 14 dB e Att = 0 dB	-9.83	3.94	-10.047	3.893
5	HGC G1 = 21 dB, G2 = 23 dB e Att = 0 dB	-9.83	11.025	-2.984	19.824
7	HGC G1 = 21 dB, G2 = 24 dB e Att = 5 dB	-14.831	6.133	-8.084	15.766
8	HGC G1 = 21 dB, G2 = 24 dB e Att = 10 dB	-19.832	1.461	-13.368	10.589
10	G1 = 19 dB, G2 = 19 dB e Att = 0 dB	-9.83	8.994	-5.005	13.815
11	G1 = 19 dB, G2 = 19 dB e Att = 5 dB	-14.831	4.03	-10.187	8.76
12	G1 = 19 dB, G2 = 19 dB e Att = 10 dB	-19.832	-0.842	-15.698	3.599

by the difference between erbium doped fiber models used in simulation and experiment since we do not have access to the intrinsic parameters of the erbium doped fiber used in the last one. Measurements accuracy also could influence on the error values. However, it is clear that the simulated results follows the same profile as the experimental results, thus confirming that the numerical results are fine tuned with the experimental.

Table 4 lists the results for both situations (without and with adaptive EDFA), for 5 and 10 dB induced of attenuation. At the initial situation, the gain of all the EDFAs were set to 14 dB, as it was enough to overcome all span losses with all channels operating below FEC limit. For a system without adaptive EDFA, only 10 Gb/s channels are properly received when a 5 dB attenuation occurs. On the other hand, for 10 dB PLI, none of the channels are below the FEC threshold. However, with adaptive EDFA, all channels for 5 and 10 dB PLI could be detected due to the better OSNR. Figures 13 (a)-(d) shows the experimental received signal constellation results for 16-QAM and DP-QPSK signals. Figs. 13 (a) and (c) present the case when a 5 dB attenuation is induced when the constellation are degraded and unable to be received. Conversely, Fig 13 (b) and (d) depict an enhancement of signal BER due to OSNR improvement performed by the adaptive EDFA algorithm for 16-QAM and DP-QPSK signals (2.94×10^{-3} and 5.46×10^{-9}, respectively). It is important to point out that non-linear compensation algorithms such as digital back propagation (DBP) or Maximum Likelihood Sequence Detection (MLSE) were not used in our bench top since for short links this enhancement given by these algorithms alone does not justify the enormous computational effort required [22].

ISSN 2179-1074

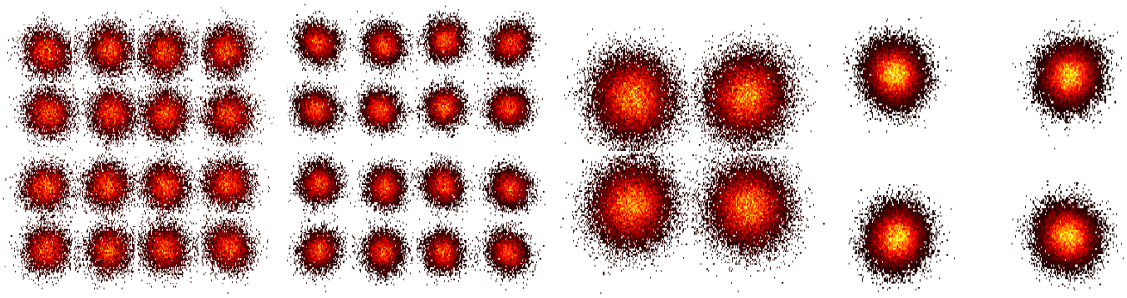

Fig. 13. Received 16-QAM and DP-QPSK signal constellation, respectively, for worst (a) and (c) and best (b) and (d) OSNR (The achieved BER 2.94×10^{-3} and 5.46×10^{-9} is within the FEC code limit).

VI. CONCLUSION

In this paper, we proposed and developed experimental-based subsystem models for EDFAs and WSSs under operation in a metropolitan optical network testbed. The results of output power for both amplifiers under test showed good agreement between simulation and experiment. In addition, all channels OSNR were also analyzed and the obtained values (bellow 1 dB) are within an acceptable margin of error. The developed sub-system method will provide greater flexibility to simulate different network scenarios and evaluate different adaptive or cognitive algorithms, thus allowing having a theoretical optical network simulation tool with components fine tuned.

ACKNOWLEDGMENT

THE AUTHORS WOULD LIKE TO THANK FUNTTEL AND CNPQ/CAPES FOR FUNDING THIS RESEARCH.

REFERENCES

[1] White paper, "Cisco Visual Networking Index: Global Mobile Data Traffic Forecast Update, 2013–2018", Feb. 2014.
[2] Van den Borne, D. et al., "Towards 400G and beyond: How to design the next generation of ultra-high capacity transmission systems," Optoelectronics and Communications Conference (OECC), pp.429-432, July 2011.
[3] Winzer, P.J., "High-Spectral-Efficiency Optical Modulation Formats," Journal of Lightwave Technology, vol.30, no.24, pp.3824,3835, Dec.15, 2012.
[4] Winzer, P.J.; Essiambre, R., "Advanced Optical Modulation Formats," Proceedings of the IEEE , vol.94, no.5, pp.952,985, May 2006.
[5] Borkowski, R., et al., "Experimental study on OSNR requirements for spectrum-flexible optical networks [Invited]," Journal of Optical Communications and Networking, vol.4, no.11, pp.B85,B93, Nov. 2012.
[6] Shankar, R. et al., "Multi-degree ROADM based on wavelength selective switches: Architectures and scalability," Optics Communications, Vol. 279, no. 1, pp.94-100, November 2007.
[7] Qusay M., "Cognitive Networks: Towards Self-Aware Networks", Wiley E-Book, New York, 2007.
[8] Melo, D. A. A., et al., "Adaptive Optical Transceivers: Concepts and Challenges", Journal of Communication and Information Systems, vol.29, no.1, May 2014.
[9] Caballero, A., et al., "Experimental demonstration of a cognitive quality of transmission estimator for optical communication systems," Opt. Express 20, B64-B70 (2012).
[10] Gonzalez, N. G., et al.. "K-means Algorithm for joint Frequency and Phase Offset Compensation in Digital Receivers for Phase-Modulated Radio-over-Fiber Links", under review in Optical Fiber Technology, 2011.
[11] Caballero, A., et al., "Cognitive, Heterogeneous and Reconfigurable Optical Networks: The CHRON Project," J. Lightwave Technol. 32, 2308-2323 (2014).
[12] Magalhães, E. C., "Global ROADM-Based Spectrum Equalizer in SDN Architecture for QoT Optimization at DWDM Networks," in Optical Fiber Communication Conference, paper W2A.35. (2014).
[13] Magalhães, E. C., " Global WSS-based Equalization Strategies for SDN Metropolitan Mesh Optical Networks," in ECOC 2014, Cannes, France, paper Tu.1.6.6, (2014).
[14] Oliveira, J., et al., "Demonstration of EDFA Cognitive Gain Control via GMPLS for Mixed Modulation Formats in Heterogeneous Optical Networks," in Optical Fiber Communication Conference/National Fiber Optic Engineers Conference , paper OW1H.2, (2013).
[15] Bjorklund, M. Ed., RFC6020 - YANG - A Data Modeling Language for the Network Configuration Protocol (NETCONF), IETF RFC, October, 2010.

received 16 May 2014; for review 20 May 2014; accepted 23 Oct 2014

ISSN 2179-1074

[16] Enns, R. Ed., M. Bjorklund, Ed., J. Schoenwaelder, Ed., A. Bierman, Ed., RFC6241 - Network Configuration Protocol (NETCONF), IETF RFC, June, 2011.
[17] Schmidt M., Lipson H. (2009) "Distilling Free-Form Natural Laws from Experimental Data," Science, Vol. 324, no. 5923, pp. 81 - 85.
[18] http://optiwave.com/products/system_overview.html.
[19] Younce R., Larikova, and Wang Y., "Engineering 400G for Colorless-Directionless-Contentionless Architecture in Metro/Regional Networks," Journal of Optical Communications and Networking (JOCN), vol. 5, no. 10, pp. A267–A273, Oct. 2013.
[20] Moura, U.C.; et al., "EDFA adaptive gain control effect analysis over an amplifier cascade in a DWDM optical system," Microwave & Optoelectronics Conference (IMOC), 2013 SBMO/IEEE MTT-S International, Aug. 2013.
[21] Savory, S.J., "Digital signal processing for coherent optical communication systems," Optoelectronics and Communications Conference and Photonics in Switching (OECC/PS), July 2013
[22] R. F. de Oliveira, J. et al,, "Hybrid EDFA/Raman Amplification Topology for Repeaterless 4.48 Tb/s (40 x 112 Gb/s DP-QPSK) Transmission Over 302 Km of G.652 Standard Single Mode Fiber," J. Lightwave Technol., v. 31, no.16, 2799-2808 (2013).

Brazilian Microwave and Optoelectronics Society-SBMO *received 16 May 2014; for review 20 May 2014; accepted 23 Oct 2014*
Brazilian Society of Electromagnetism-SBMag *ISSN 2179-1074*